L. Songsong et alii, Frattura ed Integrità Strutturale, 35 (2016) 74-81; DOI: 10.3221/IGF-ESIS.35.09

Focussed on Crack Paths

Mechanism of crack branching in the fatigue crack growth path of 2324-T39 Aluminium alloy

Lu Songsong (http://orcid.org/0000-0001-7591-434X)
Bao Rui (http://orcid.org/0000-0001-7170-082X)
Zhang Ting
Fei Binjun
Institute of Solid Mechanics, Beihang University (BUAA), 100191, Beijing, China
rbao@buaa.edu.cn

ABSTRACT. The crack growth behavior in 2324-T39 aluminium alloy was experimentally investigated. Two types of crack branching were observed. The mechanism of an uncommon crack branching which results from the link up of secondary crack with the main crack was focused on. The crack paths were observed with optical microscope and in-situ SEM. Finite element crack tip simulation was performed to investigate the relationship between plastic zone size and the location of the secondary crack. Tests and analysis results indicate that the secondary crack initiates near the plastic zone boundary and from the subsurface. The mechanism of this kind crack branching relates to the interaction of grain size and plastic zone size.

KEYWORDS. Fatigue crack growth; Crack path branching; Mechanism analysis; 2324-T39 aluminium alloy.

INTRODUCTION

Alloy 2324-T39 plate is a higher strength version of alloy 2024-T351, and is a high-purity controlled composition varient of alloy 2024. Both strength and fracture toughness properties are improved compared to 2024 plate via employing the T39 temper which was developed through special fabricating practices [1]. Since this alloy was developed for tension-dominated, fatigue and fracture critical plate applications, most of the experimental investigations about it are most focused on the fatigue crack growth and fracture. William M. [2] and Dawicke D S [3] report the fracture test results of 2324-T39 plate with difference thicknesses. Stoychev S [4] investigates the effect of varying stress intensity factor range ΔK on crack growth rate. Bao R et al. [5-7] present the macroscopic crack path branching observed during the crack growth tests of 2324-T39 middle crack tension (M (T)) specimen under spectrum loading.

According to achievements in fatigue theory and fracture mechanics, a through thickness middle crack in an isotropic thin plate subjected to remote tension-dominated loading should propagate perpendicular to the load direction, i.e., Mode I. This is reasonable from a physical perspective because the tensile stress component, which opens the crack, will certainly promote the conversion of cyclic plastic deformation into crack extension [8]. At the macro level, crack kinking, bifurcation and branching are influenced by micro-structural irregularities, load effects (global and local multiaxial stress state, spectrum loading), and environmental factors [9-13]. Though, the T39 temper was said to account for the fracture toughness improvement, there is no evidence found in the literature that the T39 temper will contribute to the macroscopic crack path change with respect to those of other Al-Cu-Mg alloys, such as 2024-T351 and 2524-T3.

In the microscopic perspective, a series of investigations on crack branching, e.g. in-situ SEM tests of a nickel-based single crystal in Ref [14] and EBSD tests on crack propagation path of 7050 alloy in Ref [15], were carried out, which suggest that the crystallographic orientations and geometry of local microstructure, particularly the tilt and twist angle, differences of slip planes or crack planes, together with cooperation and competition between movement of slip systems and loading stress influence the crack propagation behavior. Patton's research indicated that crack bifurcation may be caused by plastic anisotropy and pre-existing defects in front of crack tip [16]. Zhiyi Liu's research indicated that the extending potential decides the further extending of these bifurcated cracks [17]. The potential of the propagation concerns the tilt angle, twist angle and Schmid factor differences between two neighboring grains. These factors, of commonsense, could result in kinking, bifurcation or branching in fatigue crack path, the appearance of which could be captured as soon as it arises [18]. However, Ref. [6] reports that the crack branching observed in alloy 2324-T39 results from the linkup of secondary crack with the lead crack, the process of which is quite different from those common procedures found in the literatures, e.g. Ref. [14-18]. Ref. [7] presents the effect of overloads and ΔK level on crack path change in alloy 2324-T39.

For better understanding the mechanism of the uncommon macroscopic crack branching in 2324-T39 alloy, optical metallography analysis, in-situ SEM crack growth tests and numerical simulations on crack tip stress field were carried out in this paper, which will reveal the differences in macroscopic crack morphologies and metallographic fracture characteristics of the two types of crack branching, as well as the effect of the less common crack branching on crack growth rate and some relationship between the appearance of the less common crack branching with the crack tip plastic zone size.

EXPERIMENTS

Three kinds of crack growth tests were carried out to investigate the crack growth behavior in 2324-T39, i.e. tests with M(T) specimen of 4.5mm in thickness under spectrum loading (stated as test type I), tests with relatively small specimens of 1.5mm in thickness with single edge notch under constant amplitude loading(stated as test type II), and in-situ scanning electron microscope (SEM) crack growth tests under constant amplitude loading(stated as test type III). The details of the tests type I, such as specimen configuration, loading sequence, test procedures, etc., have been reported in Ref. [6, 7]. The aims of designing the other two kinds of tests are 1) to eliminate the potential effects of specimen thickness and loading sequence on crack branching; 2) to rule out the effect of crack configuration, i.e. middle crack and edge crack, on crack branching; 3) to observe the position where the secondary crack appears and the linkup via in-situ SEM test.

The small specimens with single edge notch used in test type II and III were cut from the aforementioned M(T) specimen. The configurations of the specimens are designed to fit the loading facilities attached to test machines, which are given in Fig. 1(a) for test type II and Fig. 1(b) for test type III. All the specimens are in L-T orientation as demonstrated in Fig. 1(c). The thickness of the specimen for test type II is 1.5mm, while it is 0.7mm for test type III.

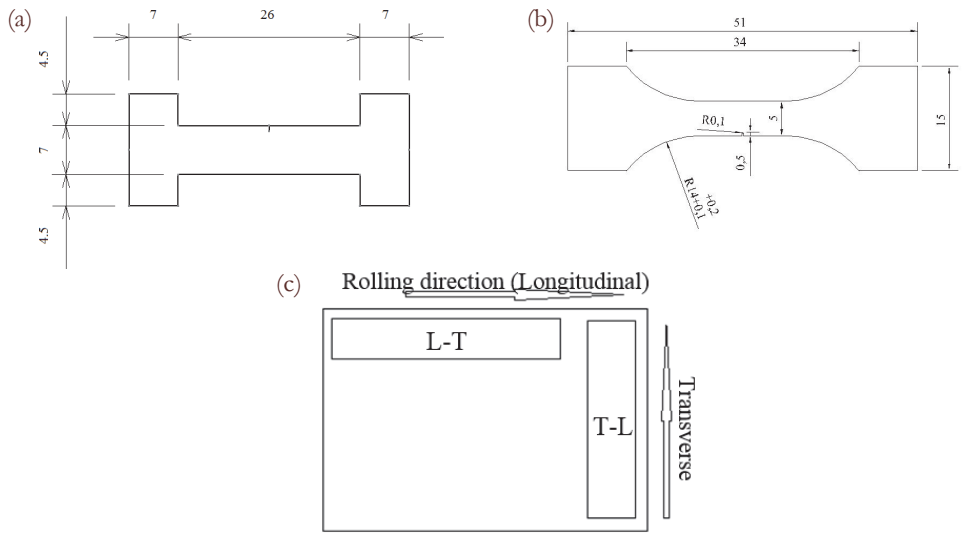

Figure 1: Specimen dimensions and orientation (Unit: mm).

Tests type II were accomplished with MTS880 servo hydraulic fatigue test system and an observation system consisting of a digital microscope, a servo motor and a raster ruler. Constant amplitude (CA) loading cycles with stress ratio R = 0.06 were employed. Two specimens, labelled as L-T-2-1 and L-T-2-2, were tested at the maximum stress σ_{max} = 140 MPa and 150 MPa, respectively. All the tests were run at 20Hz in laboratory air.

Test type III were carried out with SHIMADZU SS-550 SEM. The loading facility in the SEM is a microscopic static and dynamic testing machine produced by SHIMADZU. Constant amplitude loading cycles of R = 0.06 and σ_{max} = 150 MPa was employed in the in-situ SEM test. The test was run at 10Hz in vacuum. The specimen tested in this case is marked with L-T-3-1.

All the specimen was pre-cracked under constant amplitude load of R = 0.06 and σ_{max} = 120 MPa, which resulted in an initial crack whose length is about 0.3 mm from the notch tip.

CRACK BRANCHING PROCESS AND MECHANISM

Fig. 2(a), (b) and (c) show the crack morphologies observed in test type I, II and III, respectively. Two types of crack branching were observed in the crack paths corresponding to all the three test types. The ones marked by circle in Fig. 2 are the familiar type of crack branching which were captured once they appeared. The intersection angles are usually less than 90 degree. However, the branches marked by square in Fig. 2 are obviously different with those marked by circles. The following on discussion will centre on this type of crack branching.

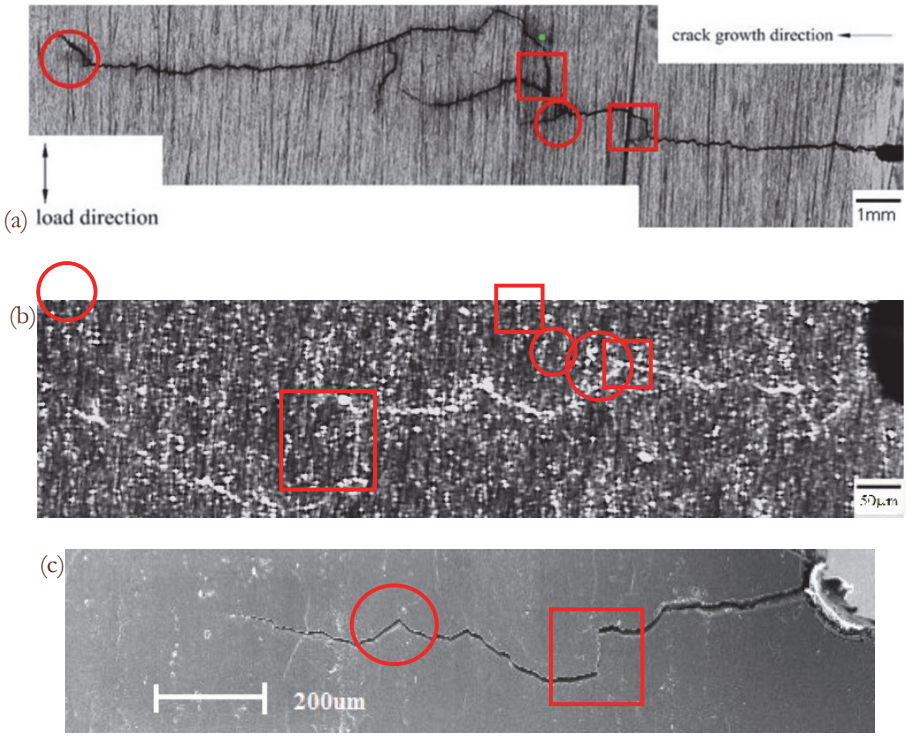

Figure 2: Crack morphologies observed in (a) M(T) specimen under spectrum loading [7], (b) single edge notch specimen (L-T-2-2) tested under CA loading, and (c) L-T-3-1 specimen tested by in-situ SEM under CA loading

It can be seen from Fig. 2, for the less familiar type of crack branching (marked by squares), the turning angles are almost 90 degree. The procedure of the appearance of such branches is also different to the common ones. The growth of the leading crack slowed down firstly, and a surface secondary crack was observed away from the leading crack tip, both of the leading crack and the secondary crack kept growing for several loading cycles and finally they linked up to each other. Fig. 3 and Fig. 4 give the observed crack branching procedures in test type I and III, respectively, which indicate exactly the same manner.

The surface secondary crack cannot be observed immediately after it initiates even in the in-situ tests. Once it appears on the specimen surfaces, it is already in a certain length as shown in Fig. 4(b). The crack growth of the secondary crack was transgranular, while the link up path was long the grain boundary. The omen of the appearance of surface secondary crack is the slowing down in the growth rate of the previously dominated crack, as shown in Fig. 5.

It can be seen from Fig. 5 that there is a remarkable crack growth rate drop at about 3467 loading cycles, however, there was no abnormal observed around the crack tip in the picture corresponding to 5969 cycles in Fig. 4(a). Compare Fig. 4(a) and (b), it can be found that there is little growth of previously dominated crack during the 2598 cycles. There is a sudden increase in crack length in Fig. 5(a) at about 8567 cycles that is because of the appearance of the surface secondary crack of about 150μm in Fig. 4(b). From these clues, it can be deduce that the secondary crack initiates from subsurface at about 3467 cycles, which dissipates the energy and in consequence decreases the growth rate of the main crack. After the link up of secondary crack and the main crack, the crack growth rate recovers.

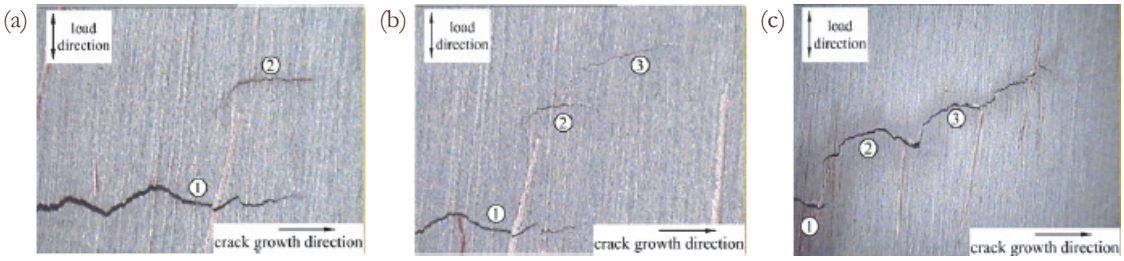

Figure 3: Appearance of secondary surface cracks and cracks linking up under spectrum loading [6].

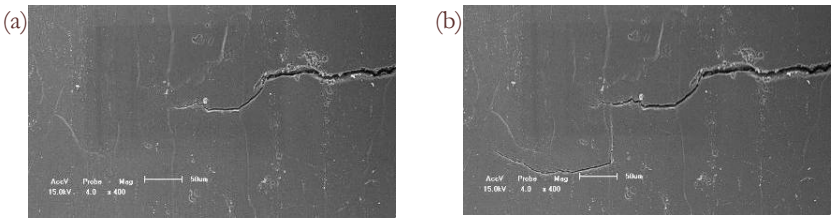

Figure 4: In-situ SEM pictures on crack path of L-T-3-1 specimen (a) at 5969 cycles and (b) at 8567 cycles under constant amplitude loading.

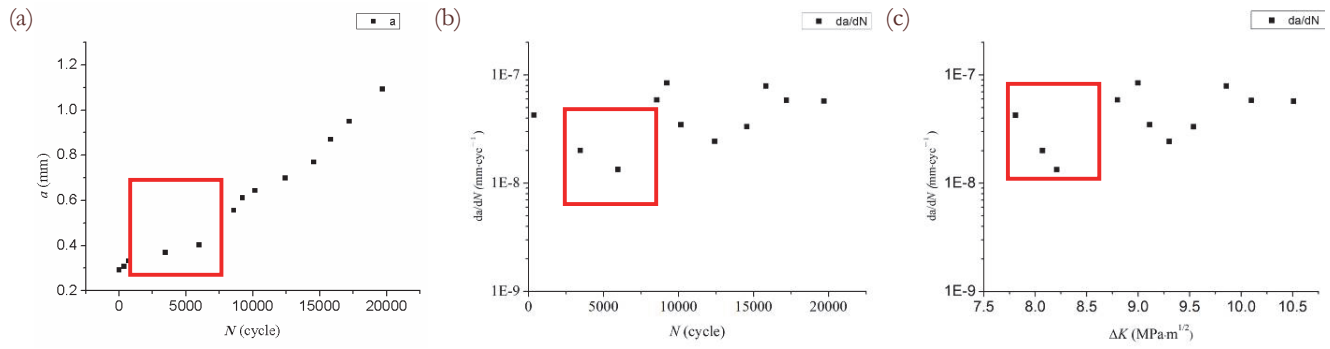

Figure 5: Crack growth data for L-T-3-1 specimen, (a) crack length *a* vs. loading cycles *N*, (b) crack growth rate d*a*/d*N* vs. loading cycles *N* and (c) crack growth rate d*a*/d*N* vs. stress intensity factor range Δ*K*

To investigate the difference in mechanism of the uncommon kind of crack branching from the common ones, optical microscope observations on the grain shape and crack growth path were carried out on the single edge notch specimen after the crack growth test.

Metallographic samples were prepared etching with Keller (1mL HF, 1.5mL HCl, 2.5mL HNO_3, 95mL H_2O) for 3 minutes after the conventional mechanical polishing to observe the grain boundary. Fig. 6(a), (b) and (c) demonstrate the microstructure on L-T, L-S and T-S metallographic planes, respectively, where S is the short transverse direction. It can be

seen from Fig. 6 that the dimension of the grains in the L direction is remarkably longer than that in the T and S direction; it looks like a layered up structure in L-S plane.

The observed crack paths in specimens L-T-2-1 and L-T-2-2, for which the applied σ_{max} are 140 MPa and 150 MPa, respectively, are given in Fig. 7 and Fig. 8.

The common type of crack branching, shown in Fig. 7(b) and Fig. 8(b), occurs at the grain boundary. For the weaker cohesion of grain boundary in this orientation, grain boundary becomes paths of easy propagation. Whereas, for the less common type of crack branching, see Fig. 7(c) and Fig. 8(c), the growth of the main crack and the surface secondary crack show transgranular characteristic, though the linkup path was along the grain boundary. Therefore, the reason for crack branching is not the weakness in grain boundaries.

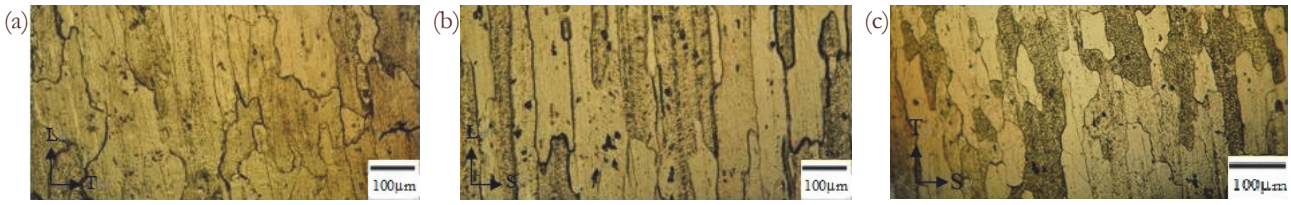

Figure 6: Grain shape observations on (a) L-T, (b) L-S, (c) T-S metallographic planes of 2324-T39 alloy.

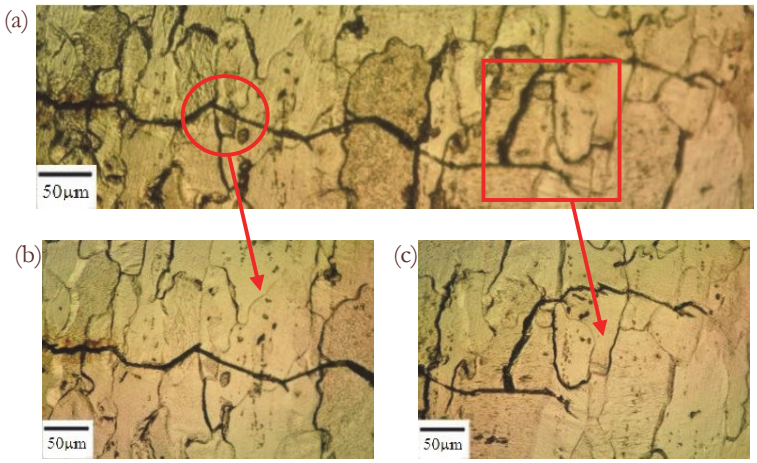

Figure 7: Crack growth path for L-T-2-1 specimen (CA loading, σ_{max} = 140 MPa, R = 0.06).

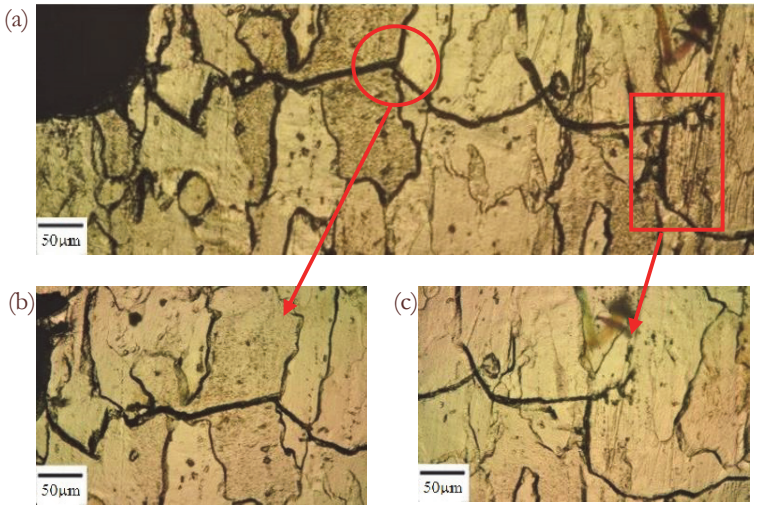

Figure 8: Crack growth path for L-T-2-2 specimen (CA loading, σ_{max} = 150 MPa, R = 0.06).

THE POSITION WHERE THE SECONDARY CRACK APPEARS

It can be seen from Fig. 2, 3, 4, 7 and 8 that the secondary cracks, on the L-T plane, located a certain distance away from the main cracks. Analysis with empirical equations and finite element (FE) simulation were performed to investigate the relationship between the value of this distance and the crack tip plastic zone size.
In the condition of small scale yielding, the curve equation of the crack tip plasticity boundaries, as shown in Fig. 9, under Mises criterion is as follows [18]:

$$r_p = \begin{cases} \dfrac{K_I^2}{2\pi\sigma_s^2}\cos^2\dfrac{\theta}{2}\left[1+3\sin^2\dfrac{\theta}{2}\right] & (\text{plane stress}) \\ \dfrac{K_I^2}{2\pi\sigma_s^2}\cos^2\dfrac{\theta}{2}\left[(1-2\nu)^2+3\sin^2\dfrac{\theta}{2}\right] & (\text{plane strain}) \end{cases} \quad (1)$$

where θ is defined as the upward inclination from the horizontal and ν is Poisson's ratio.

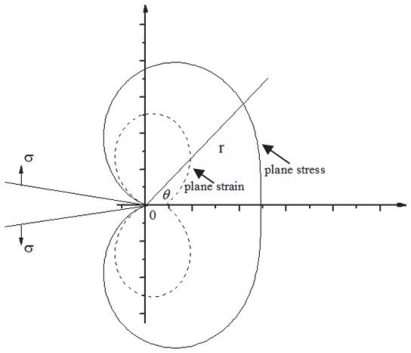

Figure 9: Sketch map of crack tip plastic zone.

It is acceptable that the crack tip is in small scale yielding state for case of the edge notch specimens used in this study when the secondary cracks initiate on the surface. Since the secondary cracks usually initiate above or below the main crack tip, θ in Eq. (1) is set to be 90 degree in the calculation. The calculation results are listed in Tab. 1 for specimen L-T-2-1, L-T-2-2 and L-T-3-1. Since the specimens are thin sheet, the calculation is based on the equation for plain stress.
Although the specimen configurations and the clapping mode were slightly different in test type II and III, the section as shown in Fig. 10(a) could be regarded as an edge cracked plane subjected to uniaxial stress state. Finite element simulation was performed for this section. Considering the symmetry, a 1/2 plane model was used here and the boundary conditions and the meshing was illustrated in Fig. 10(b) and (c). Line AB is the crack surface. Symmetry constraint was applied to line BC. Constraint in x direction and uniformly distributed load in y direction are applied to line DE.
The three specimens, i.e. L-T-2-1, L-T-2-2 and L-T-3-1, are all simulated. The widths and crack lengths of the FE models and the applied stress levels are in accord with those in the corresponding tests.
The material behavior is assumed to be elastic-plastic isotropic to acquire the crack tip stress field. The trilinear constitutive mode is adopted with σ_e = 450 MPa, $\sigma_{0.2}$ = 481 MPa, σ_b = 532 MPa, which were obtained from the σ-ε curve of the mechanical property test.

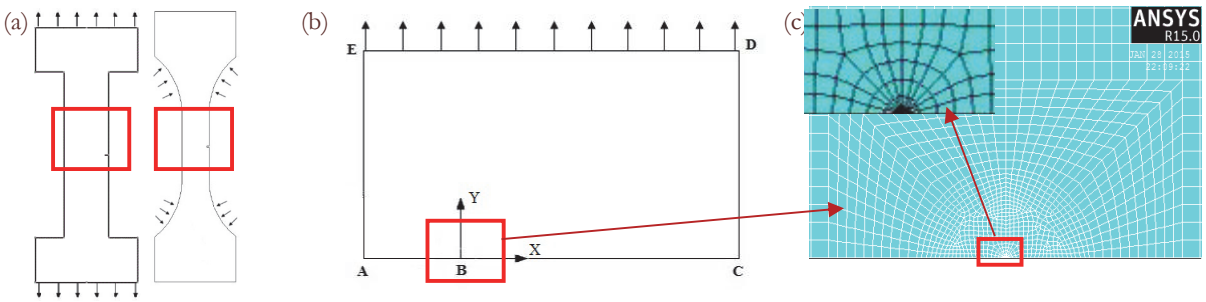

Figure 10: FE model and crack tip meshing (the meshing size of crack tip is 0.01mm).

The FE calculated plastic zone sizes at θ =90° for the three specimens are listed in Tab. 1, together with the results calculated by Eq. (1). The distances from the surface secondary cracks to the main crack tips are also measured from the optical photographs and listed in Tab. 1.
The comparison in Tab. 1 indicates that: 1) the FE simulation results are about 10% higher than the results obtained by empirical equation, that is because the elastic-plastic material model is used in the FE model; 2) the calculated plastic zone sizes at θ =90° by both Eq. (1) and FE model match the measured distances from the surface secondary cracks to the main crack tips. That is to say, the secondary cracks initiation positions are near the plastic zone boundaries of the main crack.

specimen	Measured Distance between the secondary crack and the main crack	Calculated plastic zone size of plane stress state at θ =90° by Eq. (1)	Calculated plastic zone size of plane stress state at θ =90° by FE model
L-T-1	0.241	0.209	0.23
L-T-2	0.185	0.177	0.19
L-T-3	0.083	0.074	0.08

Table 1: Comparison of the plastic zone size of plane stress state at θ =90° with the measuring distance from the secondary crack to the main crack (mm).

Conclusions

The following conclusions can be drawn from the experimental investigations and crack tip analysis:
1) The macroscopic crack branching in AA 2324-T39 results from two different types of mechanism. The uncommon kind of branching is resulted from the linking up of the secondary crack with the main crack, which is different from the intergranular crack branching.
2) The secondary cracks usually locate near the plastic zone boundaries of the main cracks and show transgranular growth characteristics. The initiation sites of the secondary cracks were deduced at the sub-surfaces of the specimen.
3) The grain shapes characteristics in different orientations of this alloy and their interaction with the plastic zone size contribute to the appearance of the second type of crack branching.

Acknowledgements

The National Natural Science Foundation of China is acknowledged for supporting the project (10802003).

References

[1] http://www.alcoa.com/mill_products/catalog/ pdf/alloy2324-t39techsheet. (2009)
[2] Johnston, W. M., Newman, Jr. J. C., Fracture Test Results for 0.5, 0.7 and 0.9 Inch Thick 2324-T39 Aluminium Alloy Material, (2001).
[3] Dawicke, D. S., Fracture testing of 2324-T39 aluminium alloy, NASA TM-109183, (1995).
[4] Stoychev, S., Kujawski, D., Mallory, J., Fatigue crack growth in 2324 aluminium alloy. MAE-05-01, (2005).
[5] Hailing, Tian, et al. Influence of low load truncation level on crack growth for Al 2324-T39 and Al 7050-T7451. Chinese Journal of Aeronautics, 22(4) (2009) 401-406.
[6] Rui, B., Zhang, X., Fatigue crack growth behaviour and life prediction for 2324-T39 and 7050-T7451 aluminium alloys under truncated load spectra, International Journal of Fatigue, 32(7) (2010) 1180-1189.
[7] Zhang, T., Rui, B., Binjun, F., Load effects on macroscopic scale fatigue crack growth path in 2324-T39 aluminium alloy thin plates, International Journal of Fatigue, 58 (2014) 193-201.

[8] Schijve, J., Fatigue of Structures and Materials, Springer, Germany, (2009).
[9] Toribio, J., González, B., Matos, J. C., Fatigue and fracture paths in cold drawn pearlitic steel. Engineering Fracture Mechanics, 77(11) (2010) 2024-2032.
[10] Beretta, S., Foletti, S., Valiullin, K., Fatigue crack propagation and threshold for shallow micro-cracks under out-of-phase multiaxial loading in a gear steel. Engineering Fracture Mechanics, 77(11) (2010) 1835-1848.
[11] Schubbe, J. J., Evaluation of fatigue life and crack growth rates in 7050-T7451 aluminium plate for TL and LS oriented failure under truncated spectra loading, Engineering Failure Analysis, 16(1) (2009) 340-349.
[12] Hénaff, G., Menan, F., Odemer, G., Influence of corrosion and creep on intergranular fatigue crack path in 2XXX aluminium alloys. Engineering Fracture Mechanics, 77(11) (2010) 1975-1988.
[13] Pook, L. P., On fatigue crack paths, International journal of fatigue, 17(1) (1995) 5-13.
[14] Zhang, Y., Shi, H.-J., Gu, J., Li, C., Kadau, K., Luesebrink O., Crystallographic analysis for fatigue small crack growth behaviors of a nickel-based single crystal by in situ SEM observation, Theoretical and Applied Fracture Mechanics, 69 (2014) 80-89.
[15] Wei, Lili, Pan, Q., Huang, H., Feng, L., Wang, Y., Influence of grain structure and crystallographic orientation on fatigue crack propagation behavior of 7050 alloy thick plate, International Journal of Fatigue, 66 (2014) 55-64.
[16] Patton, G., et al. Study of fatigue damage in 7010 aluminium alloy, Materials Science and Engineering: A 254.1 (1998): 207-218.
[17] Liu, Z., Li, F., Xia, P., Bai, S., Gu, Y., Yu, D., Zeng S., Mechanisms for Goss-grains induced crack deflection and enhanced fatigue crack propagation resistance in fatigue stage II of an AA2524 alloy, Materials Science and Engineering, A 625 (2015) 271-277.
[18] GAO Qing, Engineering fracture mechanics, Chongqing: Chongqing University Press, (1986).